King Saud University

Arabian Journal of Chemistry

www.ksu.edu.sa
www.sciencedirect.com

ORIGINAL ARTICLE

Fabrication and characterization of magnetic eucalyptus carbon for efficient Cr(VI) removal in aqueous solution and its mechanisms

Hua Zhang [a,b], Zhenyu Wu [a], Qingliang Shi [a,*], Awais Khan [c], Saeed Rad [a,b],
Asfandyar Shahab [a,b,*], Habib Ullah [d], Enas Ali [e], Ahmed A. Arafat [f],
Honghu Zeng [a,b], Liudan Luo [a,b]

[a] *Guangxi Key Laboratory of Environmental Pollution Control Theory and Technology, Guilin University of Technology, Guilin 541004, China*
[b] *Collaborative Innovation Center for Water Pollution Control and Water Safety in Karst Area, Guilin University of Technology, Guilin 541004, China*
[c] *Department of Electrical Engineering, University of Engineering and Technology, Peshawar 25000, Pakistan*
[d] *Innovation Center of Yangtze River Delta, Zhejiang University, Zhejiang 311400, China*
[e] *Faculty of Engineering and Technology, Future University in Egypt, New Cairo 11835, Egypt*
[f] *Department of Civil Engineering, College of Engineering, Taif University, P,O. BOX 11099, Taif 21944, Saudi Arabia*

Abstract   For an exhaustive removal of Cr(VI), three different types of biochar were prepared, modified and evaluated for Cr(VI) removal from wastewater. Magnetic eucalyptus biochar (MBC) was synthesized via a facile pyrolysis process of eucalyptus biochar pretreated with $FeCl_3$ firstly coupled with K_2CO_3 activation. As a comparison, raw biochar (BC) and $FeCl_3$ modified biochar (FBC) were prepared. The physicochemical property of adsorbent synthesis and removal mechanism was examined using BET, SEM with EDS, zeta potential, XRD, FTIR, XPS and Vibrating sample magnetometer (VSM), and the effect of various reaction conditions and parameters were evaluated for Cr(VI) removal. Results demonstrated that compared to BC and FBC, MBC has a larger specific surface area (870.3264 m^2/g), higher content of Fe mainly existed as γ-Fe_2O_3 and Fe_3O_4, and higher zeta potential (10.66). This is due to the significant alleviation of pore blockage caused by iron oxides and more efficient conversion of iron oxides with the participation of K_2CO_3 during modification process. Upon batch tests, the removal efficiency could

* Corresponding authors.
  E-mail addresses: shiqingliang_es@163.com (Q. Shi), 2017022@glut.edu.cn (A. Shahab).
Peer review under responsibility of King Saud University.

ELSEVIER | **Production and hosting by Elsevier**
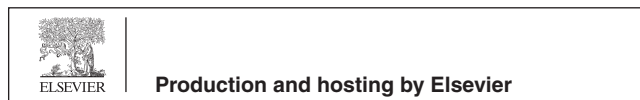
achieve more than 91% for 200 mg/L Cr(VI) solution with optimum adsorbent dosage (0.01 g) at desired acid condition (pH = 2) within 9 h. The separation behavior of MBC for Cr(VI) was highly identical with elovich and Freundlich model. MBC showed better adsorption performance up to three cycles and under various co-existing ions. Besides, the removal ability of MBC gained an obvious increase of 2–5 folds and 3–10 folds at different initial Cr(VI) concentrations, compared with BC and FBC. Characterization analyses unraveled that physicochemical removal process was responsible for the efficient elimination of Cr(VI) in an aqueous solution, resulting from adsorption, electrostatic attraction, pore filling, complexation, ion exchange, redox reaction and precipitation due to the fabrication of iron oxides into biochar.

1. Introduction

Chromium (Cr) due to its widespread uses in multiple industries, including tanning and leather industry, paint, electroplating and paper, is very common pollutant in industrial effluent. Due to its non-biodegradable and carcinogenic nature of Cr, it is quite toxic to the environment (Mo et al., 2022; Mo et al., 2021; Deng et al., 2021) and even a small content in the body (0.1 mg/g body weight) can cause severe nerve and physical damage (Lu et al., 2021). Cr mainly exists in Cr(III) and Cr(VI) form, and the latter is more toxic due to higher toxicity and mobility (Li et al., 2023; Wu et al., 2023). The metallurgy and electroplating industries in the Guilin city Guangxi Province of China produced high Cr effluent (approximately 300 mg/L), heavily threatening the local environment (Zeng et al., 2021), thus its removal is very essential.

Recently, adsorption by biochar has become an effective and widely exploited method for chromium removal owing to its easy access to raw materials, feasible preparation process, and well-endowed physicochemical properties (Mo et al., 2023; Shi et al., 2021). Nevertheless, not all pristine biochar has an excellent removal capacity for Cr(VI) in aqueous solution, especially at high concentration mainly due to its low pH_{PZC} value and limited reduction capacity (Su et al., 2021). Additionally, the difficult separation of biochar after pollutants elimination was also posed intractable restrictions for the practical application. For the targeted modification of biochar towards Cr(VI) degradation in aqueous solution, iron oxides (e.g., Fe_2O_3, Fe_3O_4) has been turned out to be greatly desirable in previous report (Acharya et al., 2021), which beneficial for the substantial improvement for the porosity and surface area of biochar and excessive introduction of adsorption sites for the significant facilitation of Cr(VI) reduction in aqueous solution (Qu et al., 2022).

Among above availably selected methods, impregnation pyrolysis is the most prevailing method for magnetic biochar preparation (Bai et al., 2021). In conventional impregnation pyrolysis process which outlined as one-step or two-steps impregnation pyrolysis, iron salt was taken as the magnetic precursor solution (e.g. $Fe(NO_3)_3$, $FeCl_2$, $FeCl_3$) to be loaded onto biomass or pyrolyzed biochar through a deep pretreatment and subsequently pyrolyzed in muffle furnace at a relatively high temperature condition (300 ∼ 1000 °C) (Yi et al., 2020). However, a solitary pretreatment method might be suffered from a low efficient load of iron salt into biomass or biochar, further leading to an inferior conversion of iron salts into iron oxides onto biochar (Zhao et al., 2022). Meanwhile, the received magnetic biochar sample might be also exhibited decaying removal performance for targeted contaminants due to blocked pores resulting from the aggregation of iron oxides (Qu et al., 2022; Zhou et al., 2018).

Thus, various modification methods were considered to be cooperative for the further enhancement of more desirable physicochemical properties, and acid or alkaline modification was demonstrated to be an effective strategy in reported work (Ma et al., 2021). However, the strong alkali agents applied for biochar modification is restricted in the wide industrial application due to its fierce reaction process and strongly corrosive effect for the reaction vessel. Compared with strong alkali, carbonate (e.g. K_2CO_3, Na_2CO_3) would be much moderate and its corrosion for the production equipment would be substantially alleviated. Moreover, in previous work, it has been proved that the activation of K_2CO_3 for biochar was vastly favorable to the development of porosity together with the significant increase of specific surface area (Wang et al., 2021). Unfortunately, rarely no attention was paid by previous report for the investigation of synergetic modification towards magnetic biochar by K_2CO_3. In this work, $FeCl_3$ was selected as the magnetic precursor and a two-steps impregnation pyrolysis method was advocated for the synthesis of magnetic biochar coupled with a synergetic modification by K_2CO_3 before the second pyrolysis process. During the pretreatment and second pyrolysis process, K_2CO_3 was reacted with eucalyptus biochar to produce CO, CO_2, H_2 and other gases, which not only proceeding the improvement of porosity and specific surface area together with an effective alleviation for the pore blockage caused by iron metal oxides but greatly profitable for the production of ferrite magnetic material (Qu et al., 2021a).

Eucalyptus is a widely planted economical tree and has advantages of large yield, fast growth, short rotation period and cheap economic effect. Owing to above superiority, eucalyptus could be picked out for the raw material for the biochar preparation. However, bulk eucalyptus biochar was not expert in the purification of Cr(VI) in aqueous solution (Zeng et al., 2021). In this report, magnetic eucalyptus biochar (MBC) was firstly fabricated through two-steps impregnation pyrolysis with pretreatment by $FeCl_3$ and K_2CO_3, followed by second pyrolysis with an appropriate heat rate before a specific period time holding. To our best knowledge, the activation by K_2CO_3 for magnetic eucalyptus biochar was rarely no perceived in previous work. To evaluate the removal performance of MBC for Cr(VI) in aqueous solution, different environmental factors, including adsorbent dosage, pH, contact time, initial concentration and reaction temperature, were comprehensively considered through a series of adsorption tests. Additionally, a series of characterization methodologies, including zeta potential, SEM, XRD, XPS and FTIR, were intensively conducted for the investigation of the physicochemical properties of resulted samples and the removal mechanism of MBC for Cr(VI).

2. Materials and methods

2.1. Materials

Raw eucalyptus materials were collected from the forest farm in Guilin, Guangxi, which were sawn into powder, subsequently rinsed, dried and ready for use. The chemical reagents applied for experiment, including ferric chloride, potassium carbonate, potassium dichromate, etc., were all in analytical purity and obtained from Xilong Scientific Co., Ltd (Shanghai, China).

2.2. Preparation of magnetic biochar

Blank biochar was prepared from above eucalyptus powder and pyrolyzed in muffle furnace at a peak temperature (400 ℃) with a heating rate of 10 ℃/min before a maintaining for 40 min. The resulted biochar sample was pulverized through 60-mesh sieve and reserved for a further modification. Subsequently, the mixture of eucalyptus biochar, K_2CO_3 and $FeCl_3$ with a weighed mass ratio of 1.5:1:1 was added in a 250 mL conical flask containing 100 mL deionized water and immersed in an oscillator for a 7 h consistent agitation at a constant temperature (55 ℃) with speed of 150 r/min to guarantee a full impregnation. The pretreated biochar was then put in a muffle furnace underwent a pyrolysis at 800 ℃ with a 60 min activation. After a post-treatment by a washing and drying process, the obtained biochar was through grinding and passing 100 mesh sieve and denoted as MBC. As a comparison, the raw biochar was exclusively modified with same dosage of $FeCl_3$ was conducted following the parallel approach, and obtained sample was marked as FBC. More details concerned about batch adsorption experiment and characterization methodologies were presented in the supplementary information (SI).

3. Result and discussion

3.1. Structure, morphology, and elemental composition of prepared materials

As shown in Table 1, the specific surface area of blank biochar (455.2956 m^2/g) is much higher than that of FBC (297.7971 m^2/g). This can be further verified in the change of surface morphology and porous structure of biochar. The smooth surface can be observed for eucalyptus biochar (Fig. S1a), while that became extremely more wrinkled together with the severe collapse and congestion of pores due to much particles being attached (Fig. S1b). Meanwhile, a significant reduction of the total pore volume and moderate increase of average pore diameter could be observed from Table 1. Additionally, the main element of Carbon and Oxygen were detected in the elemental mapping of BC, accounting for 76.76 % and 16.53 %, respectively, as shown in the EDS mass spectrum (Fig. S1c). However, Iron element was found out on the surface of FBC, with a relative high weight and atom (%) value, 15.85 and 4.09 (Fig. S1d). The decaying characteristic of biochar were mainly attributed to the severe erosion effect for the surface and pores of raw biochar due to the strong dehydrating effect of $FeCl_3$ during the modification process (Wang et al., 2022), combined with the limited introduction of iron oxides onto blank biochar surface and pores

of blank biochar (Yoon et al., 2023). These results firmly demonstrated that the single modification of $FeCl_3$ modification for eucalyptus biochar was not satisfactory, and does not totally coincided with the reported work (Wang et al., 2022; Zeng & Kan, 2022), which might be ascribed to be the more heavily destructive effect of $FeCl_3$ for the blank eucalyptus biochar (Chin et al., 2022). Noticeably, compared with FBC, the specific surface area of MBC is excessively elevated to 823.965 m^2/g, which is assigned to mesoporous carbon, even close to microporous carbon (Kumar Prajapati & Kumar Mondal, 2022). Meanwhile it was accompanied with an obvious increase of total pore volume but also little change of average pore diameter. Correspondingly, it can be observed from Fig. 1c that the pore blockage was deeply alleviated, although particles were still attached on the biochar surface and pores. Encouragingly, the content of Iron element on the biochar being significantly elevated to higher weight and atom (%) value, 16.08 and 16.53 (Fig. 2c). These results confirmed that $FeCl_3$ modification coupled with K_2CO_3 activation is a practically technical method and the K_2CO_3 agent is of vital importance for the enhancement of specific surface area and the development of total pore volume with effectively mitigating the adversely destructive effect of $FeCl_3$ agent for raw biochar. More importantly, with the assistance of K_2CO_3 activation, more iron oxides were prone to being formed onto biochar owing to the production of CO gas, whereas significantly less blockage for the biochar pores resulting from the generation of CO_2 gas, which can be further validated in the following analysis (Zhang et al., 2024). Notably, it can be seen from Table 1 that MBC underwent an obvious reduction in terms of the specific surface area and total pore volume, responding to massive particle being coated on biochar leading to severe obstruction of biochar pores (Fig. 1d). Besides, Cr was freshly detected on biochar surface (Fig. 2d), with the weight and atom (%) accounting for 6.62 and 2.40. This might to be the formation of $FeCr_2O_4$, which could be further determined in the work of Hu et al. (2024). Moreover, the content of Carbon was observed to be a drastic decline, which might to be the chemical participation of C containing functional groups for the Cr(VI) removal process (Chin et al., 2022).

In Fig. 3a, the isotherm rises to a limit value quickly with the increase of pressure, and the curve is convex and upward in the range of low relative pressure. Besides, hysteresis rings appear in the range of high relative pressure and capillary condensation occurs during adsorption. The results indicate that the N_2 adsorption–desorption isotherms of MBC remains with two types of mixing modes: I and IV and MBC has a microporous and mesoporous mixed structure (Sheha & Metwally, 2007). This can be further validated in Fig. 3b, which assigned to the fact that the pore size is mainly distributed between 3

Table 1 Physical parameters of MBC.

Sample	Multipoint BET (m^2/g)	Single-point BET (m^2/g)	Total pore volume (cm^3/g)	Average pore diameter (nm)
BC	455.2956	485.8095	0.2465	2.1655
FBC	297.7971	318.4806	0.1759	2.3632
MBC	823.965	870.3264	0.4714	2.288
MBC-Cr	707.3461	747.6413	0.4057	2.2942
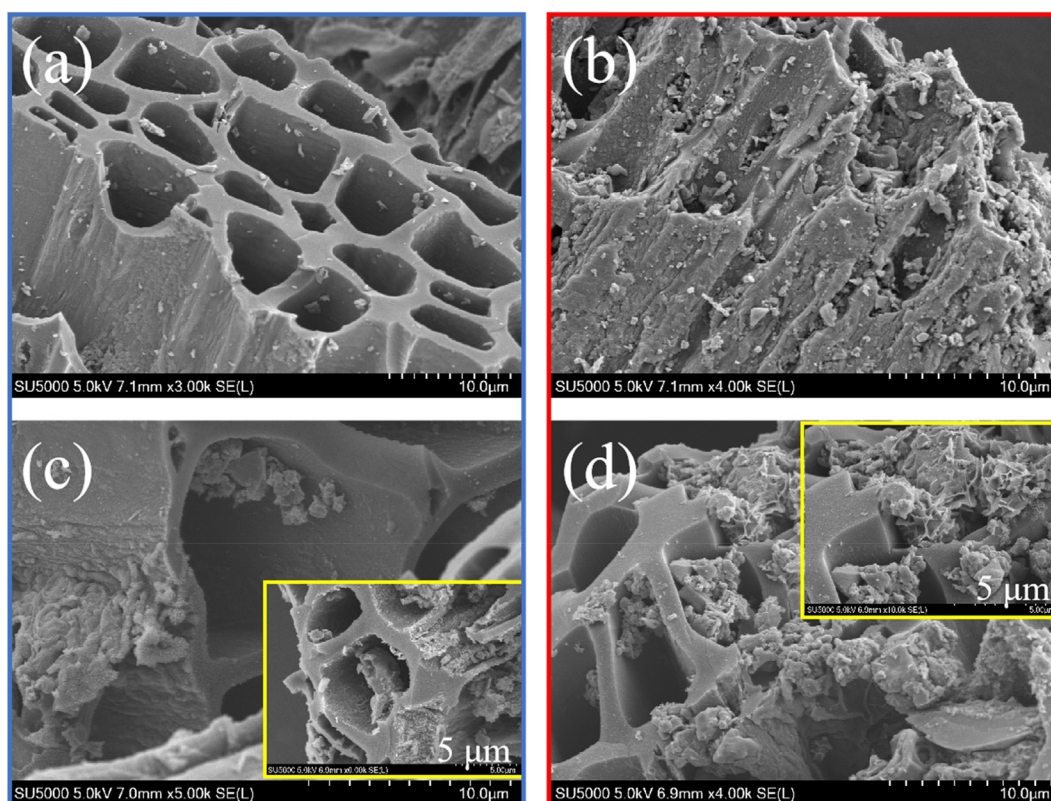
Fig. 1 SEM images of BC (a), FBC (b), and MBC before (c) and after adsorption (d).

and 10 nm. The more detailed analysis about magnetic hysteresis curves before and after adsorption was documented in Fig. S2, which could confirm its excellent magnetic property for biochar separation.

FTIR spectrum for the resulting biochar samples was exhibited in Fig. 3c. It can be seen that the main characteristic peaks of blank eucalyptus biochar are observed at 3413.386 cm^{-1}, 1598.699 cm^{-1}, 1438.636 cm^{-1} and 1384.639 cm^{-1}, which corresponding to the stretching vibration of –OH, C = O, C–C and phenolic hydroxyl functional group (–OH) (Dobrzynska et al., 2022; Zhong et al., 2021). While that for MBC, these forementioned functional groups, except the absent C–C functional group, all had a slight wavenumber movement after being modified with iron oxides and could be detected at 3413.386 cm^{-1}, 1575.577 cm^{-1}, and 1384.639 cm^{-1}, respectively. Additionally, above carbon containing functional groups of FBC was observed at 3436.571 cm^{-1}, 1628.734 cm^{-1} and 1382.711 cm^{-1}. Peaks attended at 1128.153 cm^{-1} was ascribed to the stretching vibration of O-C-O in ethers functional group, while that for FBC was found at 1116.582 cm^{-1} (Nasir et al., 2022; Wang et al., 2022). Similar phenomenon was reported in previous work (Han et al., 2022; Khalid et al., 2022). Specially, a newly emerged peak corresponding to the stretching vibration of Fe-O functional group was observed at 578.540 cm^{-1} (Yi et al., 2020), indicating that iron oxides has been successfully fabricated from the facile synthesis process with the addition of foreign iron agents. Fe-O functional group can be also identified at 490–603 cm^{-1} in previous work (Kumar Prajapati & Kumar Mondal, 2022). Specially, the peaks assigned to the Fe-O func-

tional group for FBC became much weaker and had a mild movement located at 582.397 cm^{-1}, illustrating that the solitary addition of FeCl$_3$ was not thoroughly effective for the massive introduction of iron oxides onto biochar, which identical with the prior analysis.

XRD pattern was employed for the crystalline nature analysis of resulting samples and exhibited in Fig. 3d. A large wide peak at $2\theta = 28°$, namely the amorphous diffraction peak (0 0 2), could be observed for the raw biochar, indicating its amorphous structure. The freshly present but extremely fragile diffraction peaks were observed at 2θ around 33.21°, 35.73°and 54.08°, corresponding to the lattice plan (1 0 4), (1 1 0) and (1 1 6), which assigned to the phase of hematite (α-Fe$_2$O3) (PDF#33–0664) (Min et al., 2020). Similarly reported results were also found in previous work (Li et al., 2023). However, these feeble peaks are indicated for an unsatisfactory conversion of iron oxides from the exclusive FeCl$_3$ agent, which was further validated the former analysis. Discriminatively, the newly appeared peaks attributed to the diffraction peak of (1 0 0) crystal plane of graphite structure is detected at 42.86° and 44.62°, indicating that the synthesized magnetic biochar was pertained to amorphous carbon even with the tendency of local graphitization. Additionally, freshly attentive peaks was observed at 2θ around 18.31°, 30.08°, 35.43°, 43.11°, 53.42°, 57.98° and 62.56°, which referred to the lattice plan (1 1 1), (2 2 0), (3 1 1), (4 0 0), (4 2 2), (5 1 1) and (4 4 0) of magnetite (Fe$_3$O$_4$) (PDF#19–0629) (Han et al., 2022). Furthermore, diffraction peaks which were freshly appeared at 2θ around 18.31°(1 1 1), 26.22°(2 1 1), 30.08°(2 2 0), 35.43°(3 1 1), 43.11°(4 0 0), 44.68(4 1 0), 53.42(4 2 2), 56.98°(5 1 1), and
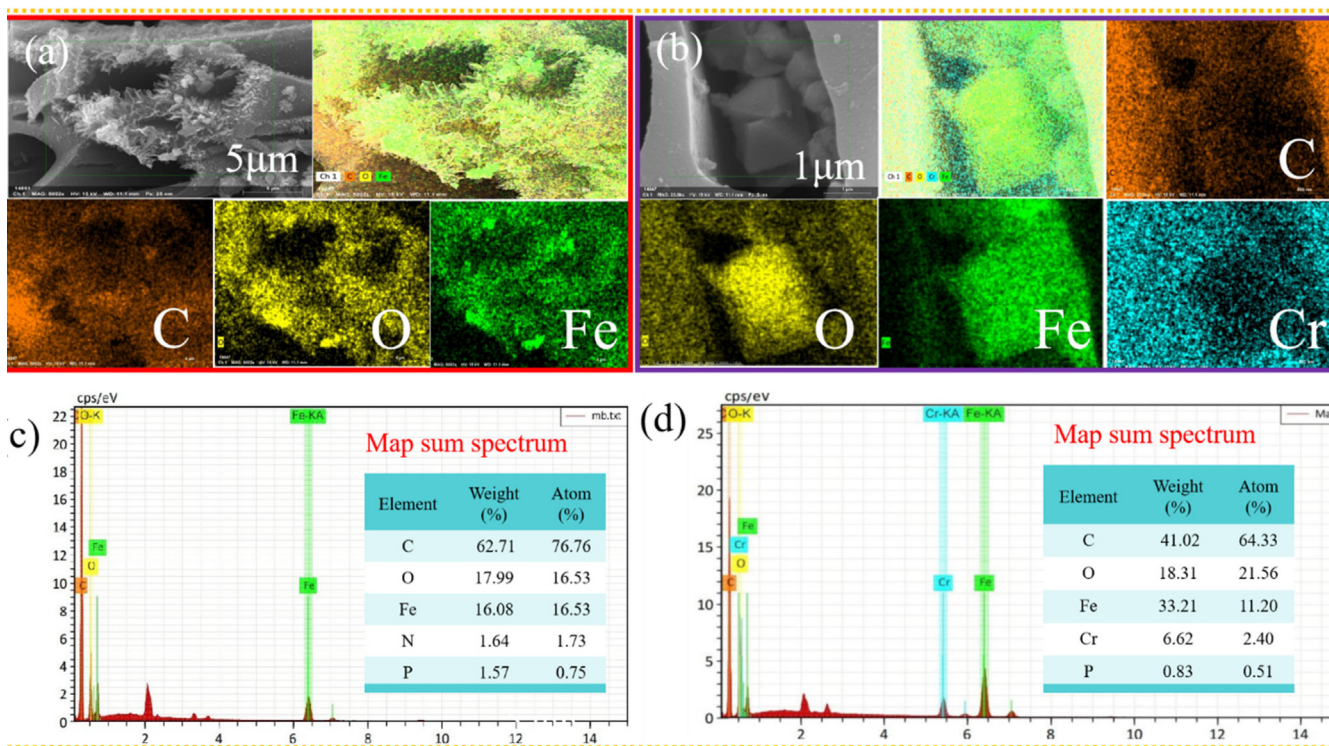
Fig. 2 The elemental mapping for MBC (a) and MBC after adsorption (b); EDS mass spectrum of MBC before (c) and after adsorption (d).

62.56°(440) could be indexed as the phase of maghemite (γ-Fe$_2$O$_3$) (PDF#39–1346) (Han et al., 2016). This detection for two iron oxides in XRD pattern was deeply evidenced the results in the FTIR analysis and highly consistent with the previous report (Fu et al., 2015). With a full impregnation of foreign agents, FeCl$_3$ and K$_2$CO$_3$ would be settled onto eucalyptus biochar and ferric oxides would be formed during the pretreatment and pyrolysis process. Owing to reducing agent C, generated ferric oxides at high temperature condition would be reduced to ferrous oxides to produce Fe$_3$O$_4$ (Zhu et al., 2022). The synthesis process can be described in following equations (Qu et al., 2022; Wang et al., 2021):

$$K_2CO_3 + 2C \rightarrow 2\,K + 3CO \tag{1}$$

$$FeCl_3 + BC \rightarrow BC\text{-}Fe(III) \tag{2}$$

$$BC \overset{\Delta\ O_2-\lim ited}{\rightarrow} CO_2 + CO + H_2 + CH_4 + \ Other\ products \tag{3}$$

$$Fe(III) - BC + CO + H_2 \rightarrow Fe_3O_4/\gamma - Fe_2O_3 - BC + CO_2\uparrow + H_2O \tag{4}$$
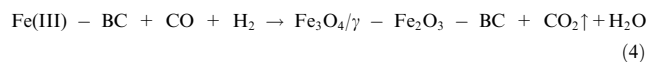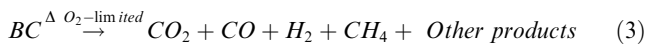
The surface composite element of MBC was investigated through XPS. In the survey spectra (Fig. 3e), apart from C and O elements, Fe element could be vividly found in biochar composites after the modification process, which deeply suggesting that iron oxide has been successfully settled onto the surface of MBC. Additionally, characteristic peaks in Fe 2p spectra could be observed at 711.51 eV and 725.20 eV, which associated with Fe$_2$O$_3$ (Fe 2p3/2) and Fe$_2$O$_3$ (Fe 2p1/2); Meanwhile, two satellite peaks located at 719.17 eV and 733.51 eV were further corroborated the appearance of Fe$_2$O$_3$ in MBC. Furthermore, two typical peaks recorded at 713.95 eV and

728.37 eV could be assigned to Fe$_3$O$_4$ (Fe 2p3/2) and Fe$_3$O$_4$ (Fe 2p1/2) (Biesinger et al., 2011; Wang et al., 2022). The obtained result was totally agreed with the analysis of XRD and FTIR and was also kept parallel with the reported work (Song et al., 2021). As shown Fig. 3g, as for C1s spectra, it could be further comprised into four peaks, denoting the carbon containing functional groups of C–C (graphitized carbon), C-OH, C-O-C, and –COOH, respectively (Wu et al., 2023). Additionally, three divided peaks in O1s plot (Fig. 3h) could be obtained at 530.60 eV, 531.97 eV and 533.63 eV, which determining the oxygen containing functional groups was presented as the form of Fe-O, C-O and C = O (Qu et al., 2021a).

pH is of vital importance for the adsorption process of magnetic biochar, not only affecting the surface charge and physicochemical properties of MBC but further determining the attentive form of the targeted contaminants (Yi et al., 2020). Consequently, the accurate measurement for the point of zero charge (pH$_{pzc}$) is highly critical for the synthesized material. It can be observed from Fig. 3i that three tested biochar material was capable of relatively high value of pH$_{pzc}$, especially for BC (pH$_{pzc}$ = 9.09), which was commonly deemed to speedily form a negative charged surface with the progressive elevation of pH in much reported work (Xing et al., 2022). This high value of BC was mainly attributed to enriched oxygen containing functional groups. Noticeably, the point of zero charge of FBC and MBC was elevated to be 10.22 and 10.66, respectively, which revealing that the introduction of iron oxides was determined to be an effective approach for improvement of biochar surface charge. Similar results were obtained in previous publications (Lu et al., 2021; Wang et al., 2019). Besides, the examined sample in this work would be easily protonated and the generated electro-
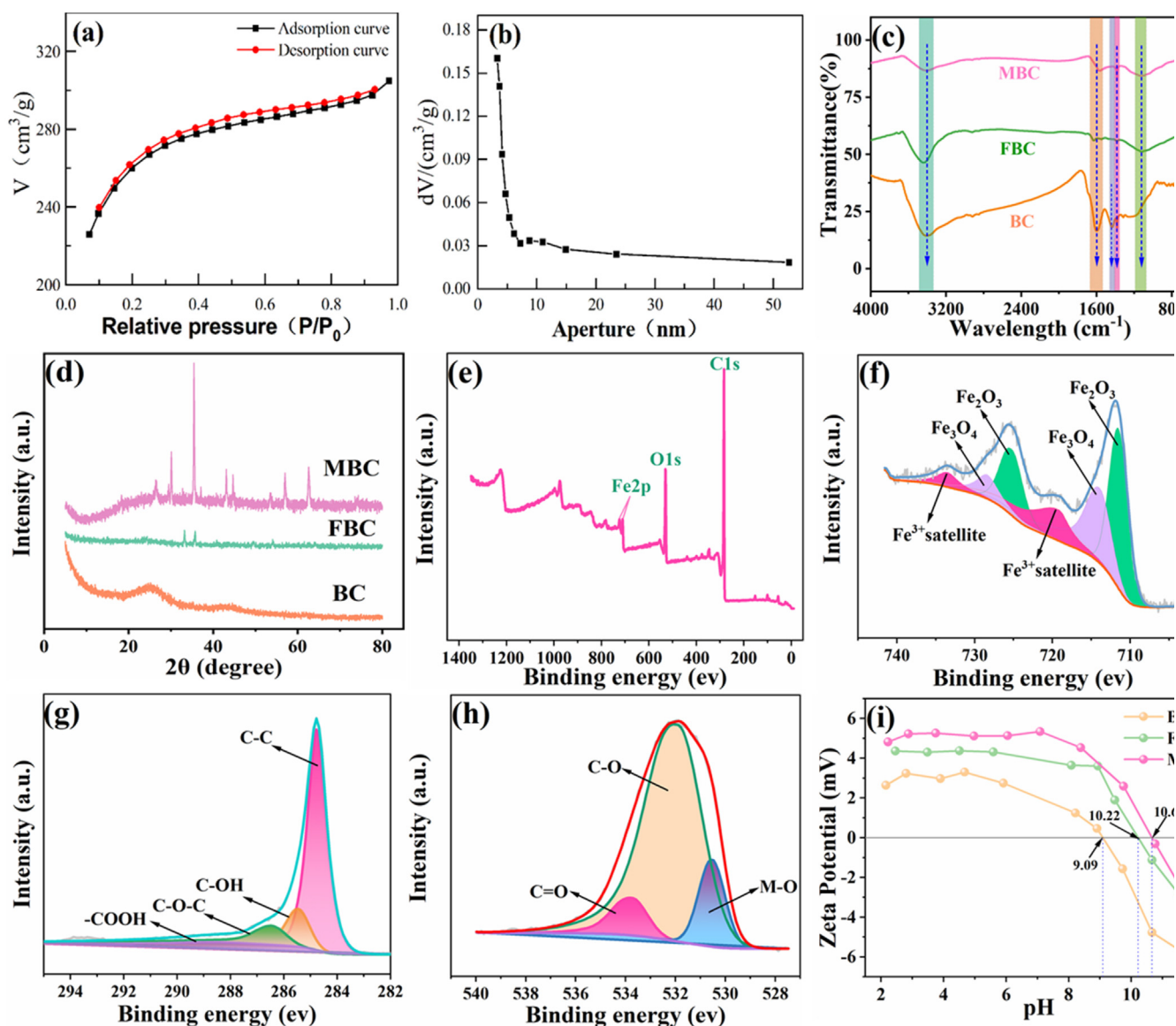
Fig. 3 N$_2$ adsorption/desorption isotherms (a), BJH pore size distributions (b), FTIR (c), XRD (d), XPS wide scans (e), high-resolution XPS of Fe (f), C (g) and O (h) plots and zeta potential (i) for MBC.

static attraction was in favor of adsorption process in the whole tested pH range, which implying that the electric repulsion force is not a key factor hindering the capture of Cr(VI) oxyanions in aqueous solution. The observed results were distinctive from much reported work considering the electrostatic attraction was the decisive role responsible for Cr (VI) removal process (Lu et al., 2021).

3.2. Influence of different environmental factors for Cr(VI) removal by MBC

3.2.1. Effect of dosage on Cr(VI) removal by MBC

The optimum MBC dosage is a key factor for the decontamination of Cr(VI) in aqueous solution, not only avoiding the thriftless adsorbent input but for the precise calculation of removal capacity. As exhibited in Fig. 4a, with MBC dosage increasing from 0 to 0.1 g, a consecutive enhancement could

be distinctly observed for removal efficiency of Cr(VI) in aqueous solution, whereas accompanied with a dramatic decline of calculated removal ability. Meanwhile, the removal efficiency of MBC was reached for a placid elevation when the MBC dosage was more than 0.1 g, which confirming an exhaustive elimination for chromium ions in aqueous solution. Commonly, adsorption sites would be more available for chromium ions in aqueous solution with a higher addition of MBC, exceedingly facilitated the efficient capture of chromium ions. Herein, the less residual chromium ions in solution would be detected and adsorption sites would not be fully exploited, resulting in higher removal efficiency but the sharp decline of calculated removal amount of Cr(VI) at per unit mass. In conclusion, 0.1 g MBC could have a satisfying removal performance for the given Cr(VI) amount in solution: the adsorption ability was 94.08 mg/g and removal efficiency was 93.99 %.

3.2.2. Effect of solution pH on Cr(VI) removal by MBC

pH is an elementary environmental factor for its far-reaching influence on Cr(VI) species and surface charge of biochar surface, which decisively determined the removal performance of biochar. In Fig. 4b, a primely satisfying removal efficiency coupled with adsorption capacity of MBC could be obviously seen at a low pH value (≤ 2). Whereas, the removal performance of MBC for Cr(VI) was extremely deteriorating along with the continuous elevation of pH value in aqueous solution especially at high pH value(≥ 3). Based on previous work, the main forms of Cr(VI) in aqueous solution are presented as $HCrO_4^-$, H_2CrO_4, $HCrO_4^-$ and $Cr_2O_7^-$ etc. (Tang et al., 2021). Besides, $HCrO_4^-$ would be the absolutely dominant species at a low pH value. Furthermore, the point of zero charge (pH_{pzc}) for biochar was 10.66. Consequently, the surfaces of MBC would be fully positively charged at a low pH condition and the protonated biochar surface is further greatly conducive to the adsorption of $HCrO_4^-$ through electrostatic attraction (Xing et al., 2022). Moreover, ferrous ions would be released in solution at a lower pH, which immensely promoted the electron transfer and reduction for Cr(VI) (Wang et al., 2020). However, the unsatisfying removal performance at a higher pH value is mainly attributed to an enormous suppression of electrostatic repulsion arising from the less positive even more negative charges being attached onto biochar surface (Qu et al., 2021b). Additionally, much more fierce competition would be occurred between OH^- and chromium ions at an increased pH owing to adsorption sites of biochar would be occupied by OH^- ions.

3.2.3. Effect of contact time on Cr(VI) removal by MBC

Reaction time is a highly crucial operation parameter for the control of the removal process along with an insightful investigation for the governing removal mechanism of Cr(VI) by MBC. As exhibited in Fig. 4c, the removal efficiency and adsorption capacity of MBC yielded up a moderate improvement with an increased reaction time. At the initial stage of adsorption, a large curve slope was implied for a fast removal process. When the reaction time exceeded 9 h, the adsorption of MBC for chromium ions in solution reached a saturated stage and the removal rate together with adsorption capacity tended to achieve a ceiling value, which were calculated as 75.55% and 75.63 mg/g, respectively. The obtained result was turned out to be that 9 h of reaction time was radically plenary for the efficient elimination of MBC for limited chromium ions in aqueous solution. Moreover, three typical kinetic equations, pseudo-first-order, pseudo-second-order, and elovich model, were applied to obtain the experimental kinetic data fitting to have a better elucidation for adsorption behavior of MBC towards chromium ions in an aqueous solution. Three kinetic equations were shown in SI.

The fitting results were presented in Fig. 4e and Table S1. Compared with pseudo-first-order model and pseudo-second order model, a higher value of R^2 was calculated as 0.9977, 0.9970 and 0.9958 for the data fitting at three tested initial Cr(VI) concentrations by elovich model. Additionally, the predicted uptake amount for Cr(VI), 66.75, 72.79 and 77.92 mg/g, was more desirable for experimental observations. These results were revealed that elovich model performed more adequately for the experimental data description, hinting that the adsorption process of Cr(VI) by MBC was mainly controlled by chemisorption. Compared with β, a much larger value of α was further implied that a rapid removal process was occurred during the early adsorption stage and modified biochar was endowed with an excellent ability for an utter purification of Cr(VI) in aqueous solution. Above drawn conclusion could be also scoured in previous work (Cheng et al., 2020). The diffusion mechanism for Cr(VI) removal was noted in SI.

3.2.4. Effect of initial concentration on Cr(VI) removal by MBC

The initial concentration of Cr(VI) in aqueous solution was the critical driving force for the mass transferring between the aqueous-solid phases during adsorption process. As depicted in Fig. 4d, it could be observed for a tardy boost of adsorption capacity (48.94–93.16 mg/g) but accompanied with an obvious reduction of removal efficiency (98.08–41.45 %) with the continuous elevation of initial Cr(VI) concentration in aqueous solution. When the initial concentration of Cr(VI) in aqueous solution at a relatively low scope, the adsorption sites on MBC surface could not be completely consumed and residual chromium ions in aqueous solution was in a small amount, resulting in a high removal efficiency yet a unsatisfying adsorbed amount for Cr(VI). Meanwhile, at a higher initial concentration of Cr(VI) in aqueous solution, the limited adsorption sites would be fully depleted and the remaining chromium ions could not be entirely captured, contributing to a harsh drop of the removal efficiency but a sluggish enhancement for the removal capacity.

To have an insightful elucidation for separation mechanism of Cr(VI) in aqueous solution by MBC, four isotherm models, including Langmuir, Freundlich, Redliche-Peterson and Temkin model, were applied for the simulation of experimental data obtained at 25 ℃ with three MBC dosage (0.05, 0.75 and 0.1 g) in Fig. 4f. The equations are shown in SI. Based on the calculated value of R^2 in Table S3, Freundlich model was a more empirical description for data fitting owing to a higher R^2 value, illustrating that non-ideal separation process of Cr(VI) by MBC occurred on a heterogeneous surface with a varied affinities and a complicated interactions involved in a physic-chemical adsorption might be accounted for the removal process (Zeng et al., 2021). Besides, the calculated value of n (0.19, 0.14 and 0.13) was in the range of 0–1, further demonstrating that the decontamination of Cr(VI) in aqueous solution by MBC was a preferential adsorption process. A relatively high value of R^2 for Temkin Model was also indicated a good data simulation behavior, which favoring that a chemical removal was involved in the adsorption process (Liu et al., 2020).

As exhibited in Fig. 4g, pH was measured after Cr(VI) removal by MBC at the saturated stage to investigate the effect of equilibrium pH on the adsorption performance. It was obviously seen that a mild elevation of pH value, which not exceeding over 0.5, was occurred after full contact of MBC with Cr(VI). The increase of equilibrium pH was resulted from the depletion of H^+ during the removal process, which was further illustrated in following analysis. Additionally, the increment of equilibrium pH was higher at low adsorbent dosage and initial concentration, which implying that redox reaction was in more participation in removal process.

To determine the feasibility of modified method, the maximum adsorption capability of BC, FBC and MBC was evalu-
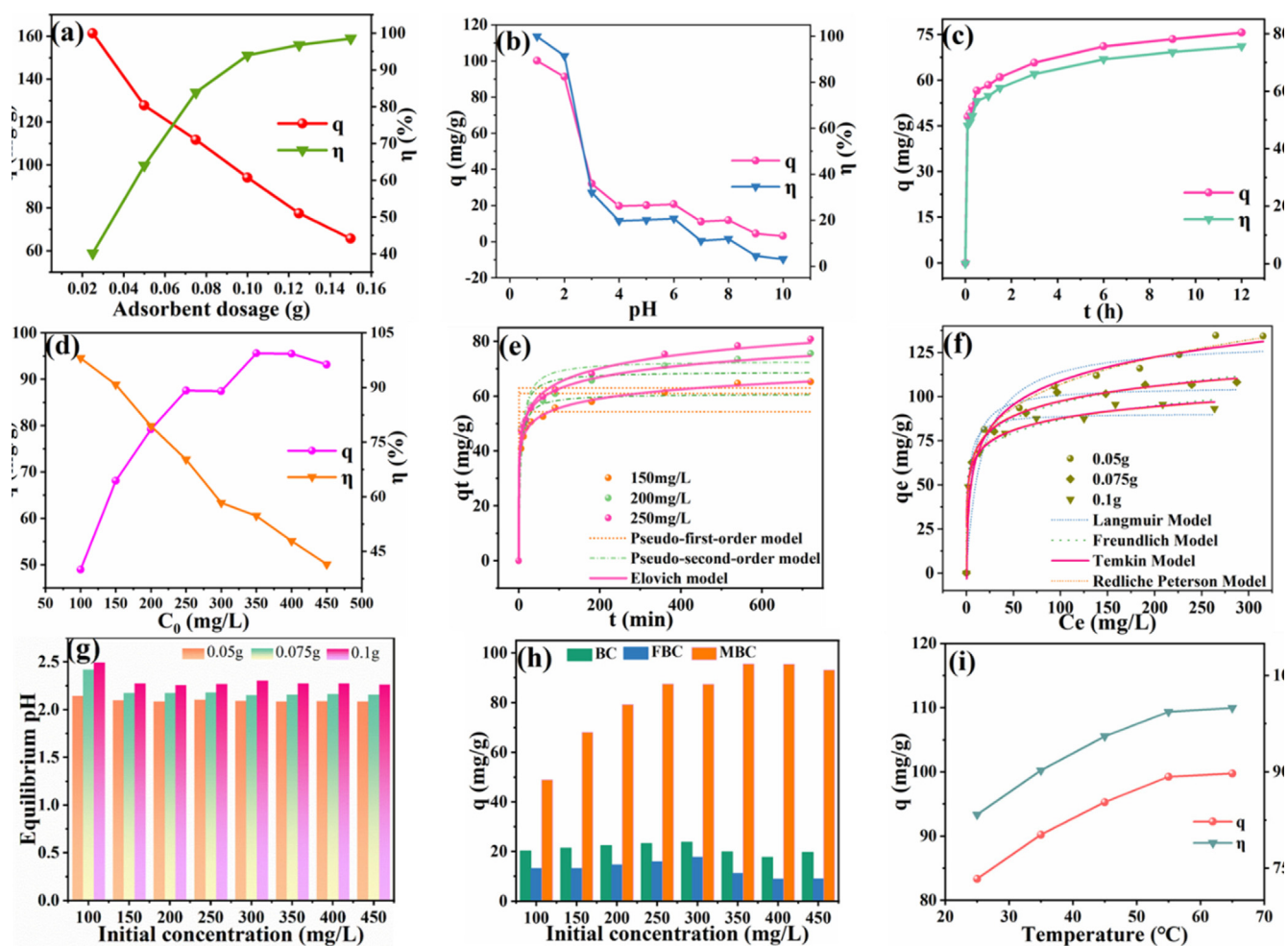
Fig. 4 Influence of environmental factors: adsorbent dosage (a), pH (b), contact time (c) and initial concentration (d); kinetic (d), isotherm (f) model for data simulation, equilibrium pH (g), comparison of adsorption capacity of material (h) and effect of temperature on Cr(VI) removal by MBC (i).

ated at high concentration of Cr(VI) in aqueous solution with 0.1 g biochar dosage (Fig. 4h). It could be observed that a significant increase of adsorption ability of 2–5 folds and 3–10 folds was achieved, compared with BC and FBC. Besides, the removal performance of MBC was absolutely more preponderant at high concentration of Cr(VI). The remarkable adsorption ability of MBC firmly demonstrated the fully competitive edge of modification method, while the unsatisfying decontamination of BC and FBC was mainly resulted from the inherently defective properties, which was illustrated in prior characterization analysis.

The purification performance for Cr(VI) in aqueous solution by some synthetized biochar was summarized in Table S4. It could be observed that the superior removal potential of MBC was determined to be much more outstanding than much reported material in previous work.

3.2.5. Effect of temperature on Cr(VI) removal by MBC

As depicted in Fig. 4i, it was evident that an uninterrupted enhancement for adsorption capacity (83.34–99.75 mg/g) and removal efficiency (83.34–99.95 %) could be observed with

the continuous rise of temperature till an adsorption equilibrium was achieved at 55 ℃. The higher reaction temperature was tremendously favorable to the increase of the molecular motion and the collision probability between adsorbate and adsorbent, thus obviously improving the adsorption of MBC for Cr(VI) in aqueous solution. Moreover, new adsorption sites might be induced due to the chemical reaction between adsorbate and functional groups on the surface of MBC especially at a the higher the temperature (Al-Othman et al., 2012).

To get a better observation for the spontaneous nature of the removal process, thermodynamic study was conducted at four initial concentrations and five given temperatures ranging from 25 to 65 ℃. Furthermore, three thermodynamic parameters, including Gibbs free energy ($\Delta G°$, kJ/ mol), standard enthalpy change ($\Delta H°$, kJ/mol) and standard entropy change ($\Delta S°$, kJ/mol), could be explained by Vant Hoff equation and the linear fitting results were shown in Fig. S4.

As listed in Table S5, it was confirmed the spontaneous and endothermic nature for the removal of Cr(VI) by MBC due to the calculated negative value of $\Delta G°$ coupled with positive value for $\Delta H°$ at operated conditions. Additionally, higher

value of $\Delta G°$ at increased temperature condition implied that the rise of reaction temperature was highly conducive to the adsorption process. The estimated value of $\Delta H°$ was determined to be more than 29 kJ/mol for the initial Cr(VI) concentration at 100 and 200 mg/L, while that was laid in 8–60 kJ/mol when the initial Cr(VI) concentration was at 300 and 400 mg/L, implying that the adsorption process was ascribed to spontaneous and endothermic chemisorption and complexation was also partially responsible for the removal of chromium ions (Duranoğlu et al., 2012). Furthermore, the positive values of ΔS was indicated the great affinity of MBC towards Cr(VI) and some structural changes during the removal process might have occurred in terms of the adsorbent and chromium species (Lin et al., 2018). Similar results were also reported in previous work for Cr(VI) removal (Xing et al., 2022).

3.2.6. Desorption and regeneration experiments

Based on the antecedent report, chromium ions can be effectively liberated from biochar surface by OH^- ions and thus NaOH with three step increased concentration (0.1, 0.2 and 0.5 mol/L) was employed as the eluent for adsorption–desorption experiments to examine the practical feasibility of MBC for Cr(VI) in aqueous solution (Lu et al., 2021). As revealed in Fig. S5b, it could be observed that the regeneration percentage of MBC underwent a mild increase in cycle 2, which achieving 43.29%, 46.95% and 53.37 % at three tested concentration of NaOH. However, at the 3rd cycle, the regeneration percentage of MBC was drastically dropped to 32.58 %, 33.34 % and 35.31 % at three different desorption solution. These results indicated that the regeneration ability of NaOH for biochar could be performed effectively within the limited cycle number, which might be due to the accumulative behavior on biochar surface and the deterioration of adsorption sites (Wang et al., 2022). The reuse potential of MBC was mentioned in Fig. S5a, which conducted in 3 cycles. It could be observed that MBC sustained a remarkable adsorption capacity at first cycle and the removal efficiency still exceeded over 97.68 %. With the consecutive operation, the removal efficiency of MBC underwent moderate reduction, but still maintained over 70 %, especially with the desorption process by higher concentration of NaOH. This might be the fact that fewer active sites were laid on biochar surface due to incomplete release by desorption process (Qu et al., 2021a; Wang et al., 2022). As a comparison, the removal efficiency of MBC drastically declined to 34.18 % with water for desorption. The result was turned out to be NaOH was in good efficiency of desorption process.

3.2.7. Effect of coexisting ions on Cr(VI) removal by MBC

As depicted in Fig. S5c, diverse interfering ions would co-exist in real aqueous environment, leading to the deteriorated purification process for targeted pollutants and thus commonly competitive ions, including Mg^{2+}, Ca^{2+}, Al^{3+}, Cl^-, SO_4^{2-}, CO_3^{2-} and PO_4^{3-}, were added to reaction system to evaluate the negative effect on MBC removal performance for Cr(VI) irrespective of the elevated high concentration (0.01–0.1 mol/L). In the mixed system, MBC exhibited a remarkable removal performance and the removal efficiency maintained at over 90 %, although acceptably decaying reduction except for the co-existing ions of Al^{3+} and PO_4^{3-}, confirming that the adsorption process by MBC was almost barely influenced. However, the removal efficiency underwent a reduction to 76.71% and 79.16 % with 0.1 mol/L Al^{3+} and PO_4^{3-}, but still relatively strong adsorption capacity. Based on reported work, the inhibitory impact of two ions for chromium ions elimination was mainly due to that the radius of tested ions was approximate to $HCrO_4^-$ species, resulting in analogous molecular size and hydration potential (Lin et al., 2018). The obtained results also supported by previous research (Kumar Prajapati & Kumar Mondal, 2022).

3.3. Investigation of potential Cr(VI) removal mechanism by MBC

3.3.1. Characterization of biochar after removal Cr(VI)

To further unravel the Cr(VI) removal mechanism by MBC, the phase changes of collected biochar samples before and after pollutants separation was identified through a series of characterization methodologies, including SEM, BET, VSM, FTIR, XRD and XPS. As exhibited in Fig. 5a, an obvious decrease of intensity after Cr(VI) removal in aqueous solution could be vividly observed for the typical peaks of Fe_3O_4 and Fe_2O_3 phase, where located at $2\theta = 30°$, $37.2°$. This result was deeply confirmed the involvement of two iron oxides for the Cr(VI) process, which could be further verified in FTIR spectra and XPS analysis. Similarly, a weakened change for peak intensity was also detected after adsorption of Cr(VI) by nanoscale zero-valent iron (nZVI) modified biochar in previous work (Dong et al., 2017). Notably, it was visible that new peaks could be freshly examined at 2θ around $30.09°$, $35.46°$, $37.05°$, $43.07°$, $53.50°$, $56.97°$ and $62.58°$ for MBC sample after removal of Cr(VI) in aqueous solution, which indexed as the lattice plan (220), (311), (222), (400), (422), (511), and (440) of chromite ($FeCr_2O_4$) (PDF#34–0140) (Fu et al., 2015). The obtained products totally coincided with prior analyses of SEM and BET and highly agreed with previous report (Zhang et al., 2018). However, a wide distinction was also laid on current work and the reported research in which oxides and hydroxides (or (oxy)hydroxides) of iron and chromium was determined to be main products of removal process (Zhao et al., 2022; Zhong et al., 2018). This might be relevant with pH value in the environment and the Fe content in the synthesized biochar composites (Zhao et al., 2022). Additionally, the resulting products were also dependent on the O_2 content in the aqueous solution because the generated electrons would be consumed by O_2 during reaction process (Nahuel Montesinos et al., 2014).

The formed chromite was mainly attributed to the involvement of iron nanoparticles during the removal process. In pH = 2 solution of Cr(VI), $HCrO_4^-$ ions could react with Fe^{2+} and were reduced to produce Cr^{3+} ions. The Cr^{3+} ions would then be partially coprecipitated to form $FeCr_2O_4$ and deposited onto biochar surface. The chemical reaction equations under acidic condition might be illustrated as follow (Zhang et al., 2019; Zhao et al., 2022):

$$3Fe^{2+} + HCrO_4^- + 7H^+ \rightarrow 3Fe^{3+} + Cr^{3+} + 4H_2O \tag{5}$$

$$Fe^{2+} + Cr_2O_4^{2-} \rightarrow FeCr_2O_4 \tag{6}$$
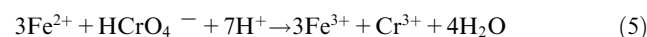
As exhibited in Fig. 5b, a marked change in FTIR spectra for MBC after adsorption of Cr(VI) could be observed for characteristic peaks of functional groups. A significant wavenumber towards a high movement could be seen for the stretching vibration absorption peak of –OH functional group located at 3418.386 cm^{-1} and vibration peak of C = O functional group observed at 1575.577 cm^{-1}. While the stretching vibration peaks of C-O-C functional group found at 1130.081 cm^{-1} was clearly noted to have a slight decrease. Above observations were indicated that chemical reaction or physical interaction occurred between functional groups on the modified biochar surface and chromium ions in aqueous solution during the removal process. Specifically, C-O-C functional group would be firstly converted into alcohol or reductive phenol and was further oxidized into C = O functional group by chromium ions accompanied with Cr(VI) being reduced to Cr(III) (Eqs.(10)-(11)), resulting in the enhancement of C = O functional groups (Zhu et al., 2018), which could be further verified in XPS analysis. Additionally, hydroxyl, carboxyl and other oxygen-containing functional groups were exposed to a large amount of positive charges owing to the protonation of biochar surface in Cr(VI) solution at a low pH value. Herein, $HCrO_4$ ions would be attached onto biochar surface through electrostatic attraction (Eqs.(8)-(9)).
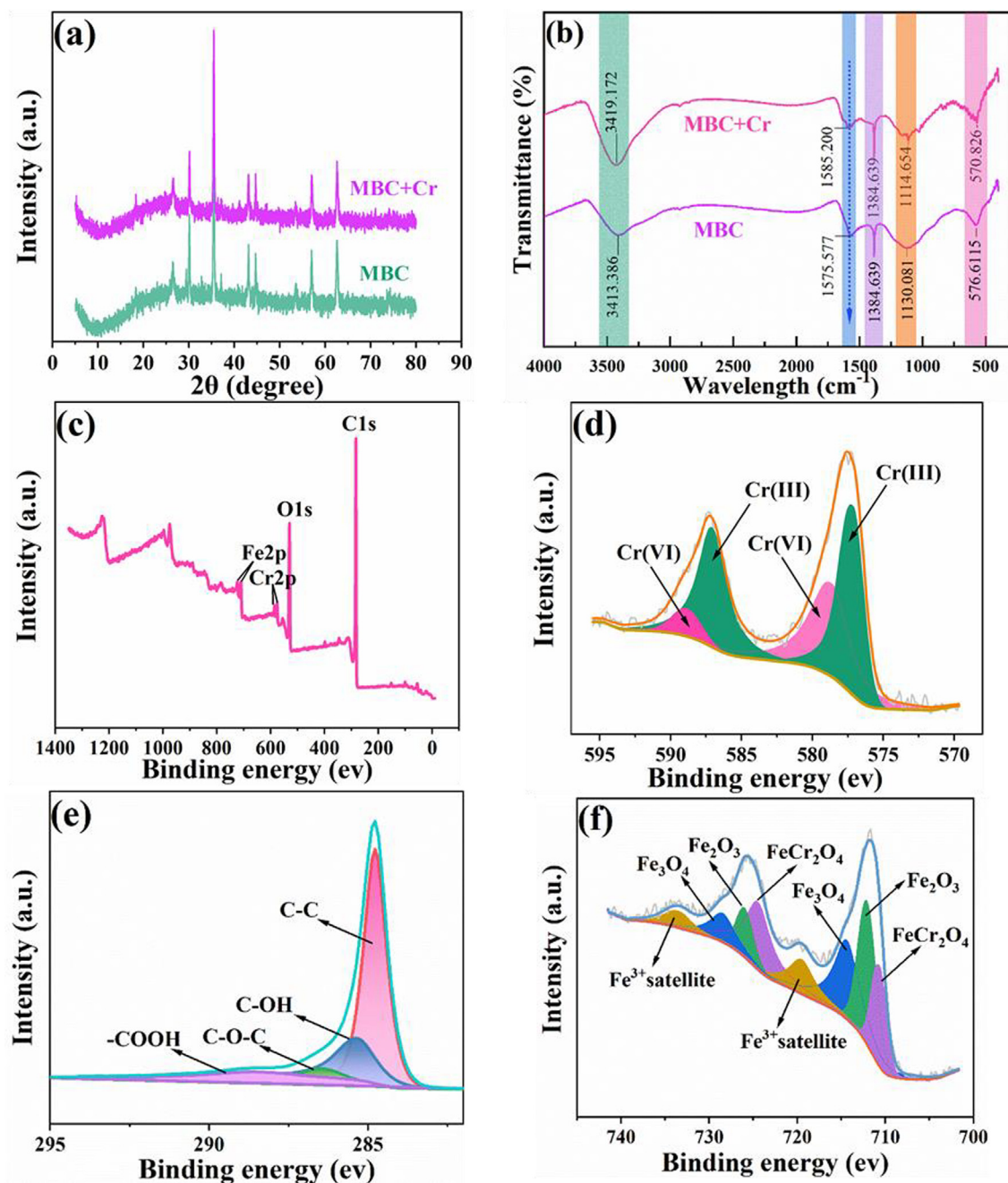
Fig. 5 Plots of XRD (a), FTIR (b), XPS wide scan (c), XPS high-resolution for Cr2p (d), C1s (e) and Fe2p (g) for MBC after Cr(VI) removal.
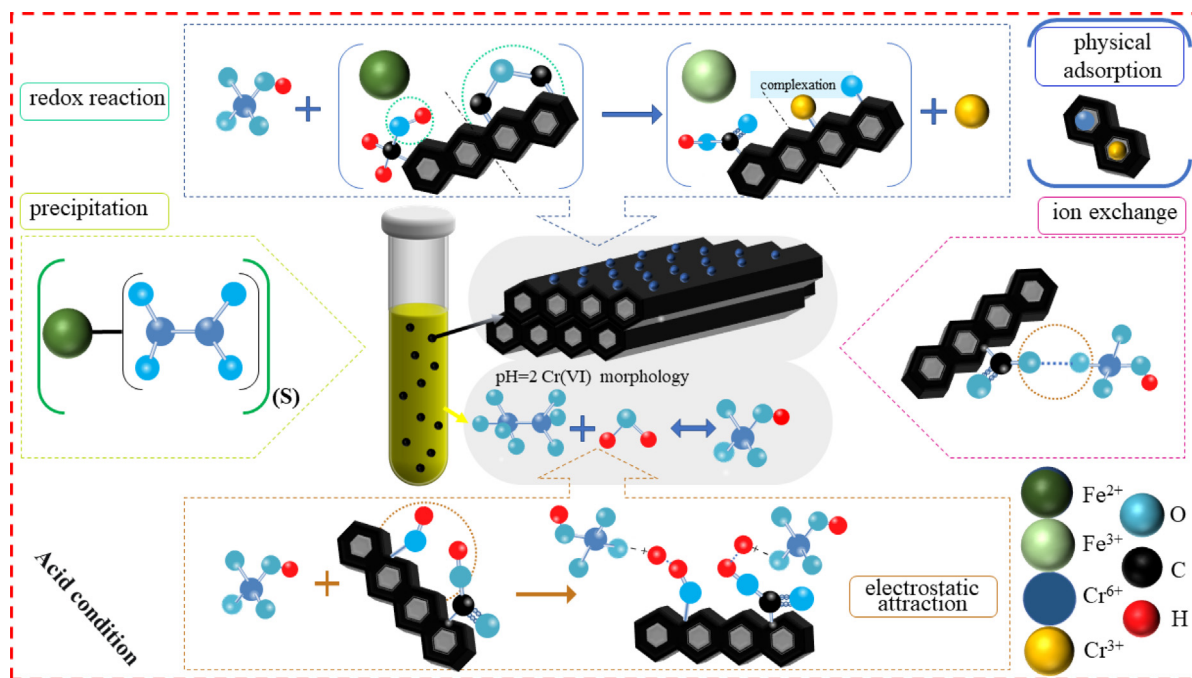
Fig. 6 Removal mechanism of Cr(VI).

Additionally, ion exchange from − COOH should not be ignored (Eqs.(12)). The possible removal mechanism was delivered by the following equations (Qu et al., 2021b):

$$Cr_2O_7^- + H_2O \leftrightarrow 2HCrO_4^- \tag{7}$$

$$R - COOH + H^+ + HCrO_4^- \rightarrow R - COOH_2^+ - HCrO_4^- \tag{8}$$

$$R - OH + H^+ + HCrO_4^- \rightarrow R - OH_2^+ - HCrO_4^- \tag{9}$$

$$3R - O - R + 3HCrO_4^- + 5H^+ \rightarrow 3R - O + 3R - Cr^{3+} + 4H_2O \tag{10}$$

$$R - CH_2OH + HCrO_4^- + 4H^+ \rightarrow R - COOH + Cr^{3+} + 3H_2O \tag{11}$$

$$R - COOH + HCrO_4^- \rightarrow R - COO^- - HCrO_4^- + H^+ \tag{12}$$
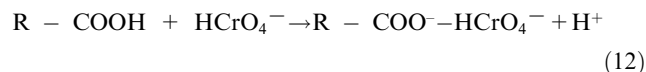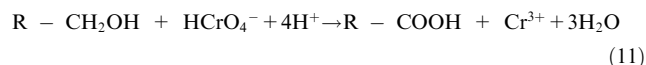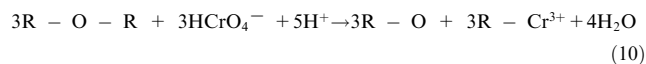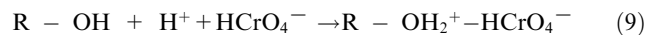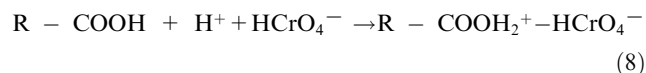
Notably, Fe-O functional group located at 576.611 cm^{-1} was recorded to have a shift towards lower position after removal process, further indicating the chemical concernment of iron oxides for the reduction of Cr^{6+} ions in solution. The obtained results were coincided with XRD analysis and compatible conclusion was drawn in Liu's report (Liu et al., 2020).

The chemical state of composites upon Cr(VI) elimination was examined through XPS to deeply probe the removal mechanism (Fig. 5c). In the survey spectrum, desired diffraction peaks, corresponding to Cr2p was newly observed together with a calculated 1.22 atomic (%) in resulted composites

(Table S6). Besides, typical peaks at 577.12 eV and 587.06 eV assigned to Cr(III) and 578.64 eV and 588.85 eV ascribed to Cr(VI) could be observed in Cr2p plot (Fig. 5d) and their atom (%) was calculated as 62.98 and 37.02 in Table S8 (Zhang et al., 2023), firmly signifying that chromium has been successfully eliminated by MBC and redox reaction was simultaneously occurred during the removal process. As shown in Table S7 and C1s spectra in Fig. 5e, it was visible that a considerable decrease of atomic for C-OH and C-O-C functional groups but an obvious rise for –COOH functional groups, accompanied with a peak position movement, could be seen upon Cr(VI) sequestration, which indicated the chemical participation of these carbon containing functional groups for the purification process. During the removal process, C-OH and C-O-C functional groups could be reacted as the reducing agent and would be further oxidized into –COOH functional group by Cr(VI) in aqueous solution (Song et al., 2021; Zhao et al., 2022), accounting for the aforementioned content change in functional groups and further validated the analysis of FTIR. Besides, the important role of C-O and C = O functional groups played in removal process could be also firmly deemed by the significant change of average atomic concentration for two functional groups in O1s plot (Fig. S6). Meanwhile, a moderate enhancement of atomic (%) for M−O functional group in O1s spectra was recorded from 13.56 to 14.20 % in Table S7, mainly resulting from the successful fabrication of Cr$_2$FeO$_4$ onto biochar surface during the adsorption process. Upon Cr(VI) separation in aqueous solution, Cr$_2$FeO$_4$ was markedly determined in Fe 2p spectra and atomic (%) (Fig. 5f) in Table S8 was highly accounted for 29.60, owing to the reduction of Fe^{2+} for Cr(VI) coupled with a coprecipitation process. This result was

greatly answered with XRD analysis and has been widely reported in previous work (Zhang et al., 2019).

3.3.2. Removal mechanism of MBC for Cr(VI)

Based on above analysis, the outstanding uptake capacity of MBC for Cr(VI) in aqueous solution was mainly dependent on physical adsorption, electrostatic attraction, complexation, redox reaction, ion exchange and precipitation under oxygen-limited/acidic condition. Schematic illustration of removal mechanism of Cr (VI) by MBC is shown in Fig. 6. Owning to easy protonation under acidic condition, chromium ions were prone to the migration towards positively charged biochar surface and rapidly adsorbed. Furthermore, attached Cr(VI) oxyanions on the biochar surface would be complexed by oxygen-containing functional groups. Secondly, redox reaction with the help of H^+ ions was occurred between functional groups, including C-OH, and -C-O-C- coupled with Fe^{2+}, and Cr(VI) in aqueous solution, resulting in Cr(VI) being converted into Cr(III) and an extensive attendance of –COOH functional group. Besides, produced Cr^{3+} ions in aqueous solution would be precipitated into Cr_2FeO_4 and further coated onto biochar surface under anoxic condition. Additionally, a portion of generated Cr^{3+} ions would be also complexed with the functional groups on the surface of biochar. Finally, the abundant pores in MBC would be filled by absorbed Cr (VI) and Cr (III).

4. Challenge and future prospect

From Fig. S7, it can be vividly observed that and the leaching amount of iron was nearly negligible when pH $\geq$ 3 and the amount of iron released from MBC in aqueous solution was adequately acceptable with the increase of pH, indicating that the magnetic stability of MBC was excellent at high pH value. However, the amount of iron dissolved from MAC was 41.31 mg/g at pH = 1 and 30.89 mg/g at pH = 2. Although MBC has been determined to be capable of excellent removal capacity for the purification of Cr(VI) in aqueous solution at low pH value, the relatively high leaching amount of iron indicates its magnetically unstable property under strong acid conditions. Herein, future work should be concentrated on the enhancement of magnetic stability of MBC at strong acid environment to broad its application and improve its repeated ability, such as introducing the carrier as an effective protection for iron oxides.

5. Conclusion

In this study, magnetic eucalyptus biochar (MBC) was successfully fabricated through two-steps pyrolysis for Cr(VI) removal in aqueous solution and its performance were compared with BC and FBC. Characterization analyses concluded that magnetic particles, γ-Fe_2O_3 and Fe_3O_4, has been coated onto eucalyptus biochar matrix with a significantly higher content of Fe element detected on surface of MBC. The addition of K_2CO_3 was more beneficial for the load of iron oxides onto biochar than the solitary $FeCl_3$ modification method. Besides, with the modification of K_2CO_3, the pore blockage was deeply alleviated, resulting in larger specific surface area (870.3264 m^2/g), compared with BC (485.8095 m^2/g) and FBC (318.4806 m^2/g). The improved physicochemical properties determined by enhanced removal ability and adsorption capacity of MBC harvested an increase of 2–5 folds and 3–10 folds at different Cr(VI) concentration, compared with

BC and FBC. Different environmental factors were figured out to have a vital influence on Cr(VI) removal by batch adsorption tests. Furthermore, the synthesized magnetic eucalyptus biochar was rendered with excellent removal ability for Cr(VI) and the adsorption behavior could be well described by elovich and Freundlich model. The outstanding removal performance of MBC for Cr(VI) was a complicated process, mainly concerned with physical adsorption and chemical adsorption arising from the participation of iron oxides and functional groups.

CRediT authorship contribution statement

Hua Zhang: Conceptualization, Supervision. **Zhenyu Wu:** . **Qingliang Shi:** Conceptualization, Methodology. **Awais Khan:** . **Saeed Rad:** . **Asfandyar Shahab:** Writing – review & editing. **Habib Ullah:** . **Enas Ali:** . **Ahmed A. Arafat:** Methodology. **Honghu Zeng:** . **Liudan Luo:** .

Declaration of Competing Interest

The authors declare that they have no known competing financial interests or personal relationships that could have appeared to influence the work reported in this paper.

Appendix A. Supplementary material

Supplementary data to this article can be found online at https://doi.org/10.1016/j.arabjc.2023.105047.

References

Acharya, R., Lenka, A., Parida, K., 2021. Magnetite modified amino group based polymer nanocomposites towards efficient adsorptive detoxification of aqueous Cr (VI): A review. J. Mol. Liq. 337.

Al-Othman, Z.A., Ali, R., Naushad, M., 2012. Hexavalent chromium removal from aqueous medium by activated carbon prepared from peanut shell: Adsorption kinetics, equilibrium and thermodynamic studies. Chem. Eng. J. 184, 238–247.

Bai, L., Su, X., Feng, J., Ma, S., 2021. Preparation of sugarcane bagasse biochar/nano-iron oxide composite and mechanism of its Cr (VI) adsorption in water. J. Clean. Prod. 320.

Biesinger, M.C., Payne, B.P., Grosvenor, A.P., Lau, L.W.M., Gerson, A.R., Smart, R.S.C., 2011. Resolving surface chemical states in XPS analysis of first row transition metals, oxides and hydroxides: Cr, Mn, Fe, Co and Ni. Appl. Surf. Sci. 257 (7), 2717–2730.

Cheng, D., Ngo, H.H., Guo, W., Chang, S.W., Nguyen, D.D., Zhang, X., Varjani, S., Liu, Y., 2020. Feasibility study on a new pomelo peel derived biochar for tetracycline antibiotics removal in swine wastewater. Sci. Total Environ. 720, 137662.

Chin, J.F., Heng, Z.W., Teoh, H.C., Chong, W.C., Pang, Y.L., 2022. Recent development of magnetic biochar crosslinked chitosan on heavy metal removal from wastewater - Modification, application and mechanism. Chemosphere 291, (Pt 3) 133035.

Deng, L., Shahab, A., Xiao, H., Li, J., Rad, S., Jiang, J. ... Siddique, J., 2021. Spatial and temporal variation of dissolved heavy metals in

the Lijiang River, China: implication of rainstorm on drinking water quality. Environ. Sci. Pollut. Res. 28, 68475–68486.

Dobrzynska, J., Wysokinska, A., Olchowski, R., 2022. Raspberry stalks-derived biochar, magnetic biochar and urea modified magnetic biochar - Synthesis, characterization and application for As (V) and Cr(VI) removal from river water. J. Environ. Manage. 316, 115260.

Dong, H., Deng, J., Xie, Y., Zhang, C., Jiang, Z., Cheng, Y., Hou, K., Zeng, G., 2017. Stabilization of nanoscale zero-valent iron (nZVI) with modified biochar for Cr(VI) removal from aqueous solution. J. Hazard. Mater. 332, 79–86.

Duranoğlu, D., Trochimczuk, A.W., Beker, U., 2012. Kinetics and thermodynamics of hexavalent chromium adsorption onto activated carbon derived from acrylonitrile-divinylbenzene copolymer. Chem. Eng. J. 187, 193–202.

Fu, R., Yang, Y., Xu, Z., Zhang, X., Guo, X., Bi, D., 2015. The removal of chromium (VI) and lead (II) from groundwater using sepiolite-supported nanoscale zero-valent iron (S-NZVI). Chemosphere 138, 726–734.

Han, Y., Cao, X., Ouyang, X., Sohi, S.P., Chen, J., 2016. Adsorption kinetics of magnetic biochar derived from peanut hull on removal of Cr (VI) from aqueous solution: Effects of production conditions and particle size. Chemosphere 145, 336–341.

Han, H., Song, P., Cai, Z., Dong, W., Khan, A., Yang, K., Fang, Y., Liu, P., Mašek, O., Li, X., 2022. Immobilizing chromate reductase NfoR on magnetic biochar reduced Cr(VI) in copper-containing wastewater. J. Clean. Prod. 361.

Hu, S., Liu, C., Bu, H., Chen, M., Fei, Y.-H., 2024. Efficient reduction and adsorption of Cr(VI) using FeCl3-modified biochar: Synergistic roles of persistent free radicals and Fe(II). J. Environ. Sci. 137, 626–638.

Khalid, W., Cheng, C.K., Liu, P., Tang, J., Liu, X., Ali, A., Shahab, A., Wang, X., 2022. Fabrication and characterization of a novel Ba2 + -loaded sawdust biochar doped with iron oxide for the super-adsorption of SO42− from wastewater. Chemosphere 303, 135233.

Kumar Prajapati, A., Kumar Mondal, M., 2022. Green synthesis of Fe3O4-onion peel biochar nanocomposites for adsorption of Cr (VI), methylene blue and congo red dye from aqueous solutions. J. Mol. Liq. 349.

Li, R., Chen, J., Zhang, H., et al, 2023. Facile synthesis of magnetic-activated nanocomposites for effective removal of cationic and anionic dyes in an aqueous environment: An equilibrium isotherm, kinetics and thermodynamic studies. Chem. Eng. Res. Des. 2023 (189), 319–332. https://doi.org/10.1016/j.cherd.2022.11.017.

Li, Y., Yin, H., Cai, Y., Luo, H., Yan, C., Dang, Z., 2023. Regulating the exposed crystal facets of alpha-Fe(2)O(3) to promote Fe(2)O (3)-modified biochar performance in heavy metals adsorption. Chemosphere 311, (Pt 1) 136976.

Lin, C., Luo, W., Luo, T., Zhou, Q., Li, H., Jing, L., 2018. A study on adsorption of Cr (VI) by modified rice straw: Characteristics, performances and mechanism. J. Clean. Prod. 196, 626–634.

Liu, L., Liu, X., Wang, D., Lin, H., Huang, L., 2020. Removal and reduction of Cr(VI) in simulated wastewater using magnetic biochar prepared by co-pyrolysis of nano-zero-valent iron and sewage sludge. J. Clean. Prod. 257.

Lu, Z., Zhang, H., Shahab, A., Zhang, K., Zeng, H., Bacha, A.-U.-R., Nabi, I., Ullah, H., 2021. Comparative study on characterization and adsorption properties of phosphoric acid activated biochar and nitrogen-containing modified biochar employing Eucalyptus as a precursor. J. Clean. Prod. 303.

Ma, Y., Qi, Y., Lu, T., Yang, L., Wu, L., Cui, S., Ding, Y., Zhang, Z., 2021. Highly efficient removal of imidacloprid using potassium hydroxide activated magnetic microporous loofah sponge biochar. Sci. Total Environ. 765, 144253.

Min, L., Zhongsheng, Z., Zhe, L., Haitao, W., 2020. Removal of nitrogen and phosphorus pollutants from water by FeCl3-impregnated biochar. Ecol. Eng., p. 149.

Mo, Z., Shi, Q., Zeng, H., Lu, Z., Bi, J., Zhang, H., Shahab, A., 2021. Efficient removal of Cd (II) from aqueous environment by potassium permanganate-modified eucalyptus biochar. Biomass Convers. Biorefin., 1–13.

Mo, Z., Tai, D., Zhang, H., Shahab, A., 2022. A comprehensive review on the adsorption of heavy metals by zeolite imidazole framework (ZIF-8) based nanocomposite in water. Chem. Eng. J., p. 136320.

Mo, Z., Zhang, H., Shahab, A., Chen, J., Huang, C., 2023. Functionalized metal-organic framework UIO-66 nanocomposites with ultra-high stability for efficient adsorption of heavy metals: Kinetics, thermodynamics, and isothermal adsorption. J. Taiwan Inst. Chem. Eng. 146, 104778.

Nahuel Montesinos, V., Quici, N., Beatriz Halac, E., Leyva, A.G., Custo, G., Bengio, S., Zampieri, G., Litter, M.I., 2014. Highly efficient removal of Cr(VI) from water with nanoparticulated zerovalent iron: Understanding the Fe(III)–Cr(III) passive outer layer structure. Chem. Eng. J. 244, 569–575.

Nasir, M., Nur, M., Pandiangan, D., Mambu, S.M., Fauziah, S., Raya, I., Fudholi, A., Irfandi, R., 2022. Phytoremediation study of water hyacinth (Eichhornia Crassipes) on zinc metal Ion (Zn2 +). Int. J. Des. Nat. Ecodyn. 17 (3), 417–422.

Qu, J., Wang, S., Jin, L., Liu, Y., Yin, R., Jiang, Z., Tao, Y., Huang, J., Zhang, Y., 2021a. Magnetic porous biochar with high specific surface area derived from microwave-assisted hydrothermal and pyrolysis treatments of water hyacinth for Cr and tetracycline adsorption from water. Bioresour. Technol. 340, 125692.

Qu, J., Wang, Y., Tian, X., Jiang, Z., Deng, F., Tao, Y., Jiang, Q., Wang, L., Zhang, Y., 2021b. KOH-activated porous biochar with high specific surface area for adsorptive removal of chromium (VI) and naphthalene from water: Affecting factors, mechanisms and reusability exploration. J. Hazard. Mater. 401, 123292.

Qu, J., Shi, J., Wang, Y., Tong, H., Zhu, Y., Xu, L., Wang, Y., Zhang, B., Tao, Y., Dai, X., Zhang, H., Zhang, Y., 2022. Applications of functionalized magnetic biochar in environmental remediation: A review. J. Hazard. Mater. 434, 128841.

Sheha, R.R., Metwally, E., 2007. Equilibrium isotherm modeling of cesium adsorption onto magnetic materials. J. Hazard. Mater. 143 (1–2), 354–361.

Shi, Q., Zhang, H., Shahab, A., Zeng, H., Zeng, H., Bacha, A.-U.-R., Nabi, I., Siddique, J., Ullah, H., 2021. Efficient performance of magnesium oxide loaded biochar for the significant removal of Pb2+ and Cd2+ from aqueous solution. Ecotoxicol. Environ. Saf. 221, 112426.

Song, J., Huang, Z., Gamal El-Din, M., 2021. Adsorption of metals in oil sands process water by a biochar/iron oxide composite: Influence of the composite structure and surface functional groups. Chem. Eng. J., p. 421.

Su, C., Wang, S., Zhou, Z., Wang, H., Xie, X., Yang, Y., Feng, Y., Liu, W., Liu, P., 2021. Chemical processes of Cr(VI) removal by Fe-modified biochar under aerobic and anaerobic conditions and mechanism characterization under aerobic conditions using synchrotron-related techniques. Sci. Total Environ. 768, 144604.

Tang, X., Huang, Y., Li, Y., Wang, L., Pei, X., Zhou, D., He, P., Hughes, S.S., 2021. Study on detoxification and removal mechanisms of hexavalent chromium by microorganisms. Ecotoxicol. Environ. Saf. 208, 111699.

Wang, Y., Miao, J., Saleem, M., Yang, Y., Zhang, Q., 2022. Enhanced adsorptive removal of carbendazim from water by FeCl3-modified corn straw biochar as compared with pristine, HCl and NaOH modification. J. Environ. Chem. Eng. 10 (1).

Wang, Z., Tian, Q., Guo, J., Wu, R., Zhu, H., Zhang, H., 2021. Co-pyrolysis of sewage sludge/cotton stalks with K2CO3 for biochar production: Improved biochar porosity and reduced heavy metal leaching. Waste Manag 135, 199–207.

Wang, X., Xu, J., Liu, J., Liu, J., Xia, F., Wang, C., Dahlgren, R.A., Liu, W., 2020. Mechanism of Cr(VI) removal by magnetic greigite/biochar composites. Sci. Total Environ. 700, 134414.

Wang, Z., Yang, X., Qin, T., Liang, G., Li, Y., Xie, X., 2019. Efficient removal of oxytetracycline from aqueous solution by a novel magnetic clay-biochar composite using natural attapulgite and cauliflower leaves. Environ. Sci. Pollut. Res. Int. 26 (8), 7463–7475.

Wu, Z., Zhang, H., Ali, E., Shahab, A., Huang, H., Ullah, H., Zeng, H., 2023. Synthesis of novel magnetic activated carbon for effective Cr(VI) removal via synergistic adsorption and chemical reduction. Environ. Technol. Innov., p. 30.

Xing, X., Ren, X., Alharbi, N.S., Chen, C., 2022. Biochar-supported Fe/Ni bimetallic nanoparticles for the efficient removal of Cr(VI) from aqueous solution. J. Mol. Liq. 359.

Yi, Y., Huang, Z., Lu, B., Xian, J., Tsang, E.P., Cheng, W., Fang, J., Fang, Z., 2020. Magnetic biochar for environmental remediation: A review. Bioresour. Technol. 298, 122468.

Yoon, K., Cho, D.W., Kwon, G., Rinklebe, J., Wang, H., Song, H., 2023. Practical approach of As(V) adsorption by fabricating biochar with low basicity from FeCl3 and lignin. Chemosphere 329, 138665.

Zeng, S., Kan, E., 2022. FeCl(3)-activated biochar catalyst for heterogeneous Fenton oxidation of antibiotic sulfamethoxazole in water. Chemosphere 306, 135554.

Zeng, H., Zeng, H., Zhang, H., Shahab, A., Zhang, K., Lu, Y., Nabi, I., Naseem, F., Ullah, H., 2021. Efficient adsorption of Cr (VI) from aqueous environments by phosphoric acid activated eucalyptus biochar. J. Clean. Prod. 286.

Zhang, G., Chen, Z., Chen, T., Jiang, S., Evrendilek, F., Huang, S., Tang, X., Ding, Z., He, Y., Xie, W., Liu, J., 2024. Energetic, bio-oil, biochar, and ash performances of co-pyrolysis-gasification of textile dyeing sludge and Chinese medicine residues in response to K2CO3, atmosphere type, blend ratio, and temperature. J. Environ. Sci. 136, 133–150.

Zhang, Y., Liu, N., Liu, P., Liu, Y., Lei, Y., 2023. Molecular-level investigation on removal mechanisms of aqueous hexavalent chromium by pine needle biochar. Arab. J. Chem..

Zhang, S., Lyu, H., Tang, J., Song, B., Zhen, M., Liu, X., 2019. A novel biochar supported CMC stabilized nano zero-valent iron composite for hexavalent chromium removal from water. Chemosphere 217, 686–694.

Zhang, S.-H., Wu, M.-F., Tang, T.-T., Xing, Q.-J., Peng, C.-Q., Li, F., Liu, H., Luo, X.-B., Zou, J.-P., Min, X.-B., Luo, J.-M., 2018. Mechanism investigation of anoxic Cr(VI) removal by nano zero-valent iron based on XPS analysis in time scale. Chem. Eng. J. 335, 945–953.

Zhao, N., Tan, X., Xiong, J., Chen, N., Gao, J., Wang, R., Yang, X., Zhang, W., Zhang, W., Qiu, R., 2022. Quantitative analysis on the redox conversion mechanism of Cr(VI) and As(III) by iron carbide based biochar composites. Chem. Eng. J., p. 446.

Zhong, M., Li, M., Tan, B., Gao, B., Qiu, Y., Wei, X., Hao, H., Xia, Z., Zhang, Q., 2021. Investigations of Cr(VI) removal by millet bran biochar modified with inorganic compounds: Momentous role of additional lactate. Sci. Total Environ. 793, 148098.

Zhong, D., Zhang, Y., Wang, L., Chen, J., Jiang, Y., Tsang, D.C.W., Zhao, Z., Ren, S., Liu, Z., Crittenden, J.C., 2018. Mechanistic insights into adsorption and reduction of hexavalent chromium from water using magnetic biochar composite: Key roles of Fe3O4 and persistent free radicals. Environ. Pollut. 243 (Pt B), 1302–1309.

Zhou, X., Zhou, J., Liu, Y., Guo, J., Ren, J., Zhou, F., 2018. Preparation of iminodiacetic acid-modified magnetic biochar by carbonization, magnetization and functional modification for Cd (II) removal in water. Fuel 233, 469–479.

Zhu, Y., Li, H., Zhang, G., Meng, F., Li, L., Wu, S., 2018. Removal of hexavalent chromium from aqueous solution by different surface-modified biochars: Acid washing, nanoscale zero-valent iron and ferric iron loading. Bioresour. Technol. 261, 142–150.

Zhu, X., Xu, Z., You, S., Komárek, M., Alessi, D.S., Yuan, X., Palansooriya, K.N., Ok, Y.S., Tsang, D.C.W., 2022. Machine learning exploration of the direct and indirect roles of Fe impregnation on Cr(VI) removal by engineered biochar. Chem. Eng. J., p. 428.